Int. J. Heat Mass Transfer. Vol. 30, No. 7, pp. 1391–1405, 1987
Printed in Great Britain

0017–9310/87 $3.00 + 0.00

Analysis of flow and heat transfer at the interface region of a porous medium

K. VAFAI and R. THIYAGARAJA
Department of Mechanical Engineering, Ohio State University, Columbus, OH 43210, U.S.A.

(*Received* 14 *August* 1986 *and in final form* 17 *November* 1986)

Abstract—Fluid flow and heat transfer at the interface region are analyzed in depth for three general and fundamental classes of problems in porous media. These are the interface region between two different porous media, the interface region between a fluid region and a porous medium, and the interface region between an impermeable medium and a porous medium. These three types of interface zones constitute a complete investigation of the interface interactions in a saturated porous medium. Detailed analytical solutions, for both the velocity and temperature distributions are derived for all of these interface conditions. The analytical temperature distributions are found in terms of confluent hypergeometric functions for two different regimes, which are found to cover almost the entire range of real fluids. The numerical and analytical results are found to be in excellent agreement. The numerical and analytical results are also checked against an empirically based hypothesis for one of the interface conditions, namely the interface between a fluid region and a porous medium, and are found to be in excellent agreement with that experimental hypothesis.

1. INTRODUCTION

THE INTERFACE region can be considered to be a boundary layer zone where the fluid flow and heat transfer characteristics of two different porous media or a porous medium and a fluid or a porous medium and an impermeable medium adjust to one another. A specific example can be cited from petroleum reservoirs wherein the oil flow encounters different layers of sand, rock, shale, limestone, etc. Similar situations are encountered in many other cases of practical interest such as geothermal operations [1, 2], nuclear waste repositories, water reservoirs, underground coal gasification, ground water hydrology, iron blast furnaces, solid matrix heat exchangers, etc. Interface interactions on flow and heat transfer present some interesting and fundamental problems which require a detailed analysis of the velocity and temperature distributions.

Most of the analytical work on fluid flow and heat transfer through porous media has been based on Darcy's law which neglects the boundary and inertial effects. The recent works which account for either one or both of these effects [3–20] stress and validate the need to take these effects into consideration, especially in heat transfer calculations.

The present study analyzes a general class of problems involving interface interactions on flow and heat transfer for three different types of interface zones. These are:

(I) interface region between two different porous media;

(II) interface region between a porous medium and a fluid;

(III) interface region between a porous medium and an impermeable medium.

The above three types of interface zones constitute a fundamental and complete investigation of the interface interactions in a saturated porous medium. Of the above three categories only the fluid mechanics of the second category has been investigated previously [21]. Prior experimental investigations on this subject were based on qualitatively justifying the assumption that the velocity gradient at the interface is proportional to the difference between the slip velocity and the Darcian convective velocity within the porous medium [21]. Furthermore, prior theoretical investigation on the second category is based on a specific and artificial mathematical model of the porous medium for which the empirically specified velocity gradient at the interface was used.

In the present work in addition to the fluid flow, the temperature distribution and the heat transfer at the interface region are analyzed in detail for all three categories. The intricacies of the boundary layer interactions at the interface on both the velocity and temperature fields are discussed in great detail and theoretical solutions are obtained for the velocity and temperature distributions as well as the interface velocity and temperature. Analytical expressions are also obtained for the Nusselt numbers for different interface conditions. Throughout the analysis, the choice of the gage parameters involved in the perturbation solutions for velocity and temperature is found to be inherently tied to the physics of the problem and therefore it is found to be very important. This leads to the use of a number of different gage functions for describing the fluid mechanics and the temperature distributions for different interfacial problems. Fur-

NOMENCLATURE

C_f fluid heat capacity [W s kg^{-1} K^{-1}]
Da Darcy number, K/L^2
F_1 a function that depends on the Reynolds number Re_1 and the microstructure of the upper porous medium, defined in ref. [3]
h channel height [m]
J unit vector aligned along the pore velocity vector, $\mathbf{V}_p/|\mathbf{V}_p|$
K permeability of the porous structure [m^2]
K_1 permeability of the upper porous medium [m^2]
L horizontal extent of the external boundary [m]
Nu Nusselt number, hx/K
P pressure [N m^{-2}]
Pr_i effective Prandtl number for the ith porous medium, ν/α_e
Re Reynolds number based on permeability of the porous medium, $\rho_f u_c K^{1/2}/\mu_f$
Re_1 Reynolds number based on permeability of the upper porous medium, $\rho_f u_{c1} K_1^{1/2}/\mu_f$
T temperature [K]
$T_{\infty,i}$ free stream temperature in the ith medium [K]
u_c Darcian convective velocity [m s^{-1}]
u_{c1} Darcian convective velocity for the upper porous medium, $-(K_1/\mu_f)(\mathrm{d}\langle P_1\rangle^f/\mathrm{d}x)$
$U_{int,A}$ interface velocity obtained from the analytical solution
$U_{int,N}$ interface velocity obtained from numerical solutions
$U_{int,exp}$ interface velocity obtained from experimental data
$\mathbf{V}$ velocity vector [m s^{-1}]
$\mathbf{V}_p$ pore velocity vector [m s^{-1}]
y_1 normal coordinate for the upper medium [m]
y_2 normal coordinate for the lower medium [m].

Greek symbols
α_e effective thermal diffusivity [m^2 s^{-1}]
α^* a proportionality constant in the Beavers and Joseph model [21]
γ porous media shape parameter, $\sqrt{(\delta/K)}$
δ porosity of the porous medium
η_{cM} non-dimensional normal coordinate for the channel region, y_1/h
η^*_{cM} non-dimensional normal coordinate for the lower medium for the case of fluid porous interface, $y_2/\sqrt{(K/\delta)}$
η_{cT} non-dimensional normal coordinate for the channel region, $y_1/\sqrt{(K/Pr_1)}$
η^*_{cT} non-dimensional normal coordinate for the porous region, $y_2/\sqrt{(K/(\delta Pr_2))}$
η_{iM} non-dimensional normal coordinate for the upper porous medium, $y_1/\sqrt{(K_1/\delta_1)}$
η_{iT} non-dimensional normal coordinate for the upper porous medium for the temperature distribution, $y_1/\sqrt{(K_1/(Pr_1\,\delta_1))}$
η^*_{iT} non-dimensional normal coordinate for the lower porous medium for the temperature distribution, $y_2/\sqrt{(K_2/(Pr_2\,\delta_2))}$
η_T non-dimensional coordinate for the porous medium
θ dimensionless temperature, $(\langle T\rangle - T_\infty)/(\Delta T)_{ref}$
λ_e effective thermal conductivity of the porous medium saturated with stagnant fluid [W m^{-1} K^{-1}]
λ_{ei} effective thermal conductivity of the ith porous medium saturated with stagnant fluid [W m^{-1} K^{-1}]
μ_f fluid viscosity [kg m^{-1} s^{-1}]
ν kinematic viscosity [m^2 s^{-1}]
ξ dimensionless horizontal length scale, x/L
ρ_f fluid density [kg m^{-3}]
σ dimensionless parameter in the Beavers and Joseph model [21].

Other symbols
$\langle\ \rangle$ 'local volume average' of a quantity.

thermore, in some cases even the scaling of the independent variable becomes crucial. A very important feature of this type of analysis is that the order of magnitude dependencies as well as the relative importance of the functional dependencies become quite evident from the solution.

The governing equations have also been solved numerically for a range of the material properties and different flow conditions. The analytical results have been found to be in excellent agreement with the numerical results. The ranges of validity of the theoretical model have been explored and their applicability discussed at length. The theoretical results are also compared with the empirically based hypothesis for the interface region between a fluid and a porous medium namely, the proportionality of the velocity gradient at the interface to the difference between the slip velocity and the Darcian velocity within the

porous medium. The agreement between these theoretical and experimental results is shown to be excellent. In addition, a detailed study on the influence of the material parameters on the interface slip velocity and the temperature distribution has been presented over a broad range of their values.

2. FORMULATION

The complexity involved in the geometric structure of a porous medium does not allow for an exact description of the velocity and temperature fields inside each individual porous structure. It has been customary to employ Darcy's law to describe the velocity field in a porous medium. While Darcy's law can be used to obtain a relation between the pressure gradient and the velocity in an unbounded porous medium for low speed flows, boundary and inertial effects can play a major role on some of the heat transfer computations. The governing momentum and energy equations, which account for the inertial and boundary effects, are given as [3–20]

$$(\rho_f/\delta)\langle(\mathbf{V}\cdot\nabla)\mathbf{V}\rangle = -\nabla\langle P\rangle^f + (\mu_f/\delta)\nabla^2\langle\mathbf{V}\rangle - (\mu_f/K)\langle\mathbf{V}\rangle - \rho_f F\delta^{1/2}[\langle\mathbf{V}\rangle\cdot\langle\mathbf{V}\rangle]J \quad (1)$$

$$\langle\mathbf{V}\rangle\cdot\nabla\langle T\rangle = (\alpha_e/\delta)\nabla^2\langle T\rangle \quad (2)$$

where μ_f is the fluid viscosity, ρ_f the fluid density, K the permeability of the porous medium, δ the porosity, $\mathbf{V}$ the velocity vector, $\mathbf{V}_p$ the pore velocity vector, $J = \mathbf{V}_p/|\mathbf{V}_p|$ the unit vector aligned along the pore velocity vector, $\langle P\rangle^f$ the average pressure read off a pressure gage, $\gamma = (\delta/K)^{1/2}$, $\langle T\rangle$ the temperature, α_e the effective thermal diffusivity defined as $\lambda_e/(\rho_f c_f)$, λ_e the effective thermal conductivity of the porous medium saturated with a stagnant fluid and c_f is the fluid heat capacity. The function F depends on the Reynolds number $Re = \rho_f u_c K^{1/2}/\mu_f$ and the microstructure of the porous medium as described in ref. [1]. Here u_c is the Darcian convective velocity in the flow direction defined as $u_c = -(K/\mu_f)\,\mathrm{d}\langle P\rangle^f/\mathrm{d}x$. Angular brackets represent the local volume averaging process. The method of local volume averaging has been discussed in detail by Whitaker [22, 23]. An order of magnitude analysis on the momentum equation shows that the momentum boundary layer thickness is of the order of $(K/\delta)^{1/2}$ and that the convective term $\langle(\mathbf{V}\cdot\nabla)\mathbf{V}\rangle$ causing boundary layer growth is significant only over a length of the order of (Ku_c/ν) [3, 4]. The latter quantity is small for most practical situations. Therefore, a fully developed momentum boundary layer results beyond a very short developing length. For this case, the momentum equation (1) reduces to [3, 4, 6]

$$(\mu_f/\delta)\nabla^2\langle\mathbf{V}\rangle - (\mu_f/K)\langle\mathbf{V}\rangle - \rho_f F\delta^{1/2}\gamma[\langle\mathbf{V}\rangle\cdot\langle\mathbf{V}\rangle]J - \nabla\langle P\rangle^f = 0. \quad (3)$$

This work is primarily concerned with the analysis of fluid flow and heat transfer through an interface zone composed of at least one porous medium. For the problem under study, the velocity field in the porous medium will be independent of the flow direction and the system of governing equations inside the porous medium reduces to [13]

$$(\mu_f/\delta)\,\mathrm{d}^2\langle u\rangle/\mathrm{d}y^2 - (\mu_f/K)\langle u\rangle - \rho_f F\delta^{1/2}\gamma\langle u\rangle^2 - \mathrm{d}\langle P\rangle^f/\mathrm{d}x = 0 \quad (4)$$

$$\langle u\rangle\partial\langle T\rangle/\partial x = (\alpha_e/\delta)\partial^2\langle T\rangle/\partial y^2. \quad (5)$$

Considering the momentum equation (4), the first term represents the viscous resistance offered by the boundary to the flow. The second and third terms which form a linear combination of the flow velocity and the square of the flow velocity, are a measure of the frictional resistance offered by the structure of the porous body. The last term, the pressure gradient along the flow direction, is thus seen to balance the inertial and viscous resistances encountered by the flow outside the boundary layer. Thus the boundary and inertial effects are both considered in this formulation. The energy equation (5) describes a balance between the convected energy, directly influenced by the fluid flow and the energy diffusion normal to the flow direction, effected by the heat conduction process.

The present work considers fluid flow and heat transfer for the general class of interfacial problems which includes the interface between two different porous media or the interface between a porous medium and a fluid or the interface region between a porous medium and a solid boundary. These three fundamental types of the interfacial problems are shown in Fig. 1. Despite the fact that there is a discontinuity of material properties at the interface, the fluid flow and the temperature fields need to satisfy conditions of smoothness in this zone. More specifically, the velocity and temperature fields and the shear stress and heat flux distributions should be continuous across the interface in order to be physically meaningful. The present formulation accounts for both boundary and inertial effects and the continuity conditions.

3. FLUID FLOW ANALYSIS AT THE INTERFACE

As discussed before the general class of the interfacial problems in saturated porous media consists of three fundamental categories. In this section the fluid mechanics of each of these categories will be investigated in depth.

3.1. *Fluid mechanics of the interface region between different porous media*

The problem under study consists of two layers of porous media with a common interface between them. Figure 1(a) shows the schematic of the problem. To analyze the problem the velocity field is nondimensionalized on the basis of the characteristic Dar-

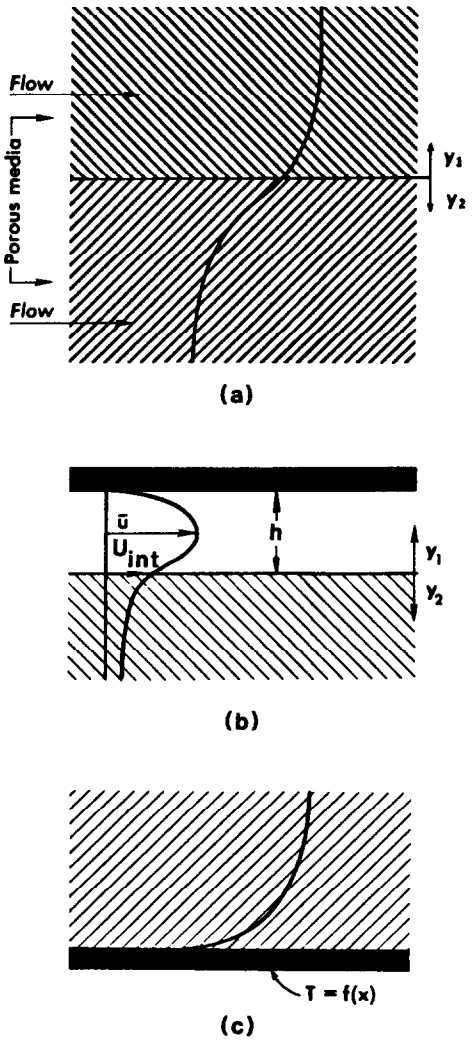

FIG. 1. (a) The interface region between two different porous media. (b) The interface region between a porous and a fluid region. (c) The interface between an impermeable medium and a porous medium.

cian convective velocity u_{ci} as $u_i = \langle u \rangle_i / u_{ci}$ where $\langle u \rangle_i$ is the velocity in the ith porous medium and $u_{ci} = -(K_i/\mu_f)\,\mathrm{d}\langle P_i \rangle^f/\mathrm{d}x$, and the subscript i refers to the properties and parameters of the ith porous medium.

The qualitative velocity profile includes a boundary layer region at the interface where the two different velocity fields of the two porous media adjust to each other. In what follows, singular perturbation analysis is used to obtain an analytical solution for the velocity profiles in the interface region. These velocity profiles are then used to obtain an explicit expression for the interface velocity in terms of the material properties of the two media. The momentum equation (4) for the two porous media reduces to

$$(K_i/\delta_i)\,\mathrm{d}^2u_i/\mathrm{d}y^2 - u_i - \beta_i\delta_i u_i^2 + 1 = 0 \qquad (6)$$

where $\beta_i = F_i Re_i$. The solution for this equation can be found in terms of a cumbersome equation. For this reason we have chosen to abandon that solution in favor of the matched asymptotic expansions which would reveal a lot more of the physics of the problem. Since $(K_i/\delta_i)^{1/2} \ll 1$, the velocity field attains a constant value far from the interface, in both porous media. The velocity field in the interface region corresponds to the inner solution and the constant free stream values for the velocity correspond to the outer solution to equation (6). The solution procedure involves the use of the common, unknown interface velocity as a boundary condition to solve for the velocity fields in each porous medium near the interface. This unknown interface velocity is determined by employing conditions of continuity of velocity and shear stress across the interface.

The velocities u_i are expanded in terms of powers of the porosities δ_i as

$$u_i = u_i^0 + \delta_i u_i^1 + \delta_i^2 u_i^2 + \ldots \qquad (7)$$

The outer solution u_{*1} for the upper porous medium can be easily seen to be

$$u_{*1} = 1 - \beta_1\delta_1 + 2\beta_1^2\delta_1^2 - 5\beta_1^3\delta_1^3 + \ldots \qquad (8)$$

The solutions for the first three orders of the inner solution for the upper porous medium are found to be

$$u_1^0 = 1 + (U_0^0 - 1)\exp(-\eta_{iM}) \qquad (9)$$

$$u_1^1 = U_0^1 \exp(-\eta_{iM}) + \beta_1(-1 + \exp(-\eta_{iM}) \times (1 - \eta_{iM}(U_0^0 - 1) - (U_0^0 - 1)^2/3) + \exp(-2\eta_{iM})(U_0^0 - 1)^2/3) \qquad (10)$$

$$u_1^2 = U_0^2 \exp(-\eta_{iM}) + \beta_1 U_0^1(-\exp(-\eta_{iM}) \times (\eta_{iM} + 2(U_0^0 - 1)/3) + 2\exp(-2\eta_{iM}) \times (U_0^0 - 1)/3) + \beta_1^2(2 + \exp(-\eta_{iM}) \times (A_1\eta_{iM}^2 + B_1\eta_{iM} + C_1) + \exp(-2\eta_{iM}) \times (D_1\eta_{iM} + E_1) + \exp(-3\eta_{iM})(U_0^0 - 1)^3/12) \qquad (11)$$

where

$$A_1 = (U_0^0 - 1)^2/2 \qquad (12)$$

$$B_1 = (U_0^0 - 1)^2/3 + 3(U_0^0 - 1)/2 - 1 \qquad (13)$$

$$C_1 = 5(U_0^0 - 1)^3/36 + 2(U_0^0 - 1)^2/3 - 2(U_0^0 - 1)/3 - 2 \qquad (14)$$

$$D_1 = -2(U_0^0 - 1)^2/3 \qquad (15)$$

$$E_1 = 2(U_0^0 - 1)/3(1 - (U_0^0 - 1) - (U_0^0 - 1)^2/3) \qquad (16)$$

and $\eta_{iM} = y_1/\sqrt{(K_1/\delta_1)}$ is the non-dimensional normal coordinate for the upper medium.

Typically, for the upper porous medium the inner solution, given by equations (7) and (9)–(11), can be seen to match with the outer solution given by equation (8) as the inner variable, η_{iM}, goes to infinity.

An explicit expression for the interface velocity is

found from the inner solutions for the two porous media, employing conditions of continuity across the interface. This interface velocity is solved in terms of ratios of material properties and parameters of the two porous media, such as permeability, porosity, friction factor and pressure gradients [24]. The comparisons between the theoretical and numerical interface velocities are given in the discussion section.

3.2. *Fluid mechanics of the interface region between a porous medium and a fluid*

Here the problem consists of a porous medium exposed to a fluid layer as depicted in Fig. 1(b). In this case the governing equation in the channel region is simple and is given by the simplified Navier–Stokes equation. The solution for the channel flow is found to be

$$u_{c1} = U_0 + \eta_{cM}(1-U_0) - \eta_{cM}^2 \tag{17}$$

where η_{cM} is a non-dimensional length variable for the channel region given by y_1/h, where h is the channel height, and U_0 is the unknown interfacial slip velocity.

In the porous medium introducing the gage parameter

$$\varepsilon_{cM} = \sqrt{\left(\frac{K}{\delta}\right)}\frac{1}{h} \tag{18}$$

the governing equation becomes

$$h^2\varepsilon_{cM}^2\frac{d^2u_{c2}}{dy_2^2} - u_{c2} - \alpha u_{c2}^2 + 2\delta\sigma\varepsilon_{cM}^2 = 0 \tag{19}$$

where $\alpha = F\delta Re$, $Re = (u_{ch}\sqrt{K})/\nu$ and $u_{c2} = \langle u\rangle_2/u_{ch}$. Since the true characteristic Darcian velocity in the porous medium is much smaller than the characteristic velocity in the channel, u_{c2} is expanded as

$$u_{c2} = \varepsilon_{cM}u_1 + \varepsilon_{cM}^2u_2 + \varepsilon_{cM}^3u_3 + \ldots \tag{20}$$

The inner equation for the porous medium can be written from equation (19) as

$$\frac{d^2u_{c2}}{d\eta_{cM}^{*2}} - u_{c2} - \alpha u_{c2}^2 + 2\delta\varepsilon_{cM}^2 = 0 \tag{21}$$

where η_{cM}^* is the non-dimensional normal coordinate for the lower medium given by $y_2/\sqrt{(K_2/\delta_2)}$. The first three orders of the inner solution for the porous section are found to be

$$u_1 = \exp(-\eta_{cM}^*) \tag{22}$$

$$u_2 = 2\delta - \left(\frac{2}{3}\alpha + 1\right)\exp(-\eta_{cM}^*) + \frac{\alpha}{3}\exp(-2\eta_{cM}^*) \tag{23}$$

$$u_3 = \left[(1-2\delta) + \frac{5}{3}\alpha + \frac{23}{36}\alpha^2 + 2\alpha\delta\left(-\eta_{cM}^* - \frac{1}{2}\right)\right]\exp(-\eta_{cM}^*) - \frac{2}{3}\alpha\left(\frac{2}{3}\alpha + 1\right)\exp(-2\eta_{cM}^*) + \frac{\alpha^2}{12}\exp(-3\eta_{cM}^*). \tag{24}$$

The unknown U_0 is then found from the channel and inner solutions, equations (17) and (22)–(24). Direct comparison between the theoretical and the experimental as well as numerical results is given in the discussion section.

3.3. *Fluid mechanics of the interface region between a porous medium and an impermeable medium*

The interface region for this part is shown in Fig. 1(c). The solutions for the first three orders of inner velocity components are found to be much simpler for this case and are given by

$$u_1^0 = 1 - \exp(-\eta_{iM}) \tag{25}$$

$$u^1 = \beta\left[-1 + \exp(-\eta_{iM})\left(\frac{2}{3} + \eta_{iM}\right) + \frac{1}{3}\exp(-2\eta_{iM})\right] \tag{26}$$

$$u^2 = \beta^2\left[\left(\left(2 - \eta_{iM}^2 + \frac{13}{3}\eta_{iM} + \frac{29}{18}\right)\Big/2\right) \times \exp(-\eta_{iM}) - \left(\left(2\eta_{iM} + \frac{10}{3}\right)\Big/3\right)\exp(-2\eta_{iM}) - \exp(-3\eta_{iM})/12\right] \tag{27}$$

and where $\eta_{iM} = y_1/\sqrt{(K_1/\delta_1)}$, is, as before, the non-dimensional coordinate into the porous medium.

4. HEAT TRANSFER ANALYSIS AT THE INTERFACE

In this section analytical expressions are obtained for temperature distributions for all interface conditions. The governing energy equation in a porous medium is given by equation (5). In obtaining an analytical expression for the temperature distribution it is crucial to account for the different temperature and velocity boundary layer thicknesses.

4.1. *Temperature distribution at the interface region between a porous medium and an impermeable medium*

The physical problem is shown in Fig. 1(c). The energy equation can be written as

$$u\frac{\partial\theta}{\partial\xi} = \frac{K/\delta}{Re\,Pr\sqrt{Da}}\frac{\partial^2\theta}{\partial y^2}. \tag{28}$$

In general the temperature at the boundary is a function of ξ which is the dimensionless horizontal length scale, x/L, therefore, the boundary conditions for this case are taken as

$$\theta(0, y) = 0$$
$$\theta(\xi, 0) = f(\xi) \tag{29}$$
$$\theta(\xi, y \to \infty) = 0$$

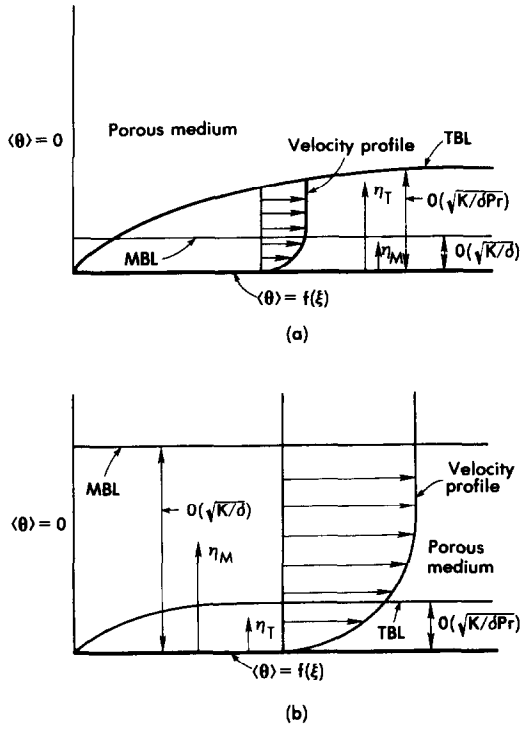

FIG. 2. (a) Comparison between the MBL and TBL for low Prandtl number fluids. (b) Comparison between the MBL and TBL for high Prandtl number fluids.

where θ is the dimensionless temperature distribution given by $(\langle T\rangle - T_\infty)/(\Delta T)_{ref}$ where $(\Delta T)_{ref}$ is some reference temperature related to the temperature difference between the interface and the core of the porous medium, Da the Darcy number, K/L^2, and Pr the Prandtl number, ν/α_e. As mentioned previously the differences between the momentum and thermal boundary layers should be fully accounted for in the analysis. The viscous boundary layer (MBL) is of constant thickness and is of the order of $\varepsilon_M = \sqrt{(K/\delta)}$. The thermal boundary layer (TBL) will be of the order of $\varepsilon_T = \sqrt{((K/\delta)/Pr)}$. Two limiting cases will now be considered.

Case I. Low Prandtl number fluids

The analysis for this case is composed of two physically distinct regions in the fluid flow regime (see Fig. 2(a)). These are the region inside the TBL but outside the MBL and the region inside the MBL. Physically these regions are so distinct that they have to be treated separately.

Inside the MBL. The normal coordinate is scaled as $\eta_M = y/\varepsilon_M$ and in the limit of $Pr \to 0$, the temperature distribution is derived to be

$$\theta(\xi, \eta_M) = f(\xi)$$

thus showing that the MBL region is essentially transparent to the boundary condition at the impermeable wall.

Outside the MBL. The normal coordinate is scaled as $\eta_T = y/\varepsilon_T$. In this region, the velocity field attains its free stream value U_∞ which is found to be

$$U_\infty = \frac{-1+\sqrt{(1+4\beta\delta)}}{2\beta\delta} \tag{30}$$

where $\beta = F\,Re$.

Thus the energy equation and boundary conditions are written as

$$\Omega\frac{\partial\theta}{\partial\xi} = \frac{\partial^2\theta}{\partial\eta_T^2} \tag{31}$$

$$\theta(0, \eta_T) = 0$$

$$\theta(\xi, \eta_T \to \infty) = 0 \tag{32}$$

$$\theta(\xi, 0) = f(\xi).$$

Here

$$\Omega = U_\infty\, Re\sqrt{Da}.$$

Taking a general form for the variation of the boundary temperature as

$$f(\xi) = A\xi^p \tag{33}$$

the solution for the energy equation is obtained in terms of the parabolic cylinder function D_{-2p-1} as

$$\theta(\xi, \eta_T) = A\Gamma(p+1)\left[2^{p+1/2}\pi^{-1/2}\xi^p \times \exp\left(-\frac{\Omega\eta_T^2}{8\xi}\right)D_{-2p-1}\left(\sqrt{\left(\frac{\Omega\eta_T^2}{2\xi}\right)}\right)\right]. \tag{34}$$

Comparison between this theoretical result and the numerical solution is given in the discussion section.

Case II. Large Prandtl number fluids

Here the thermal boundary layer is completely inside the momentum boundary layer (see Fig. 2(b)). Therefore, the region inside the TBL requires a smaller scale than the region inside the MBL but outside the TBL.

Outside the TBL. The normal coordinate is scaled as $\eta_M = y/\varepsilon_M$ and in the limit of $Pr \to \infty$, it can be shown that the temperature distribution corresponds to the free stream temperature boundary condition, i.e.

$$\theta(\xi, \eta_M) = 0.$$

Inside the TBL. The normal coordinate is scaled as $\eta_T = y/\varepsilon_T$. The velocity distribution, very close to the impermeable wall and inside the TBL is found to be linear and given by

$$u(\eta_T) = \left(1 - \frac{\beta\delta}{3} + \frac{4\beta^2\delta^2}{9}\right)Pr^{-1/2}\eta_T. \tag{35}$$

The energy equation and the corresponding boundary conditions can be written as

$$\lambda\eta_T\frac{\partial\theta}{\partial\xi} = \frac{\partial^2\theta}{\partial\eta_T^2} \tag{36}$$

$$\theta(0, \eta_T) = 0$$

$$\theta(\xi, 0) = f(\xi) \tag{37}$$

$$\theta(\xi, \eta_T \to \infty) = 0$$

where

$$\lambda = \left(1 - \frac{\beta\delta}{3} + \frac{4\beta^2\delta^2}{9}\right) Re\sqrt{(Da/Pr)}.$$

The final temperature distribution for this case is obtained in terms of the Whitaker function

$$\theta(\xi, \eta_T) = \frac{3^{1/2}\Gamma(p+1)\Gamma(2/3)}{2}\left(\frac{\lambda\eta_T^3}{9\xi}\right)^{-1/3}(A\xi^p) \times \exp\left(-\frac{1}{2}\frac{\lambda\eta_T^3}{9\xi}\right) W_{-p-1/3,1/6}\left(\frac{\lambda\eta_T^3}{9\xi}\right) \quad (38)$$

where W denotes the Whitaker function and Γ denotes the gamma function.

4.2. *Temperature distribution at the interface region between two porous media with different free steam temperatures*

The temperature fields in the two porous media in the interface region are nondimensionalized as

$$\theta_{i1} = \frac{\langle T_1\rangle - T_{\infty,1}}{T_{\infty,2} - T_{\infty,1}}$$

and

$$\theta_{i2} = \frac{\langle T_2\rangle - T_{\infty,2}}{T_{\infty,1} - T_{\infty,2}}$$

where $T_{\infty,1}$ and $T_{\infty,2}$ are the free stream temperatures in the upper and lower porous media, respectively. The unknown interface temperature $\langle T_i\rangle$ is written as

$$\theta_{i1}(\xi, 0) = \Delta(\xi) = \frac{\langle T_i\rangle - T_{\infty,1}}{T_{\infty,2} - T_{\infty,1}}$$

$$\theta_{i2}(\xi, 0) = \nabla(\xi) = \frac{\langle T_i\rangle - T_{\infty,2}}{T_{\infty,1} - T_{\infty,2}}.$$

The interface temperature, used as a boundary condition, is solved using continuity conditions across the interface.

Case I. Low Prandtl number fluids

The basic components of this case are composed of four distinct regions in the flow field. These are: two regions in the upper and lower porous media which are inside the MBL, and two regions in the TBL but outside the MBL in the upper and lower porous media. Again, it can be shown that the temperature distribution inside the MBL regions is constant and equals the interface temperature. The temperature distributions in the upper and lower porous media inside the TBL are obtained in terms of the complementary error functions

$$\theta_{i1}(\xi, \eta_{iT}) = [1 + (r_1 r_2 r_5 r_6)^{1/2}]^{-1} \times \operatorname{erfc}\left(\frac{1}{2}\sqrt{\left(\frac{\Omega_1\eta_{iT}^2}{\xi}\right)}\right) \quad (39)$$

$$\theta_{i2}(\xi, \eta_{iT}^*) = [1 + (r_1 r_2 r_5 r_6)^{-1/2}]^{-1} \times \operatorname{erfc}\left(\frac{1}{2}\sqrt{\left(\frac{\Omega_2\eta_{iT}^{*2}}{\xi}\right)}\right) \quad (40)$$

where $r_1 = K_1/K_2$, $r_2 = \delta_1/\delta_2$, $r_5 = \lambda_{e1}/\lambda_{e2}$, and $r_6 = \Omega_1/\Omega_2$ are the ratios of material properties and parameters of the two porous media. Here

$$\Omega_1 = \left[\frac{\sqrt{(1 + 4F_1\, Re_1\, \delta_1)}}{2F_1\delta_1} - 1\right]\sqrt{Da_1} \quad (41)$$

$$\Omega_2 = \left[\frac{\sqrt{(1 + 4F_2\, Re_2\, \delta_2)}}{2F_2\delta_2} - 1\right]\sqrt{Da_2}. \quad (42)$$

Dimensionless coordinates η_{iT} and η_{iT}^* for the upper and the lower porous media are respectively given by $y_1/\sqrt{(K_1/Pr_1\,\delta_1)}$ and $y_2/\sqrt{(K_2/Pr_2\,\delta_2)}$. It is found that for low Prandtl number fluids even though the temperature profiles do change as we move downstream, the interface temperature is invariant with ξ. This situation is analogous to the transient contact heat conduction problem, for which the temperature profiles do change as a function of time, while the interface temperature remains constant. As it will be shown in the next section, the situation is quite different for the high Prandtl number fluids.

Case II. High Prandtl number fluids

For this case, the analysis for the region inside the TBL becomes quite involved. However, outside the TBL region the temperature distributions in the two media attain the free stream temperature values. Inside the TBL region, the velocity distribution is linear and the governing equation for the upper porous medium is derived to be

$$(\psi_1 + \Lambda_2\eta_{iT}\, Pr_1^{-1/2})\frac{\partial\theta_{i1}}{\partial\xi} = \frac{\partial^2\theta_{i1}}{\partial\eta_{iT}^2} \quad (43)$$

where

$$\psi_1 = U_0\, Re_1\sqrt{Da_1} \quad (44)$$

$$\Lambda_2 = \left[(1 - U_0^0) - \left[U_0^1 + \frac{\beta_1}{3}((U_0^0)^2 + U_0^0 + 1)\right]\delta_1 - \delta_1^2\left[U_0^2 + \frac{\beta_1 U_0^1}{3}(2U_0^0 + 1) + \frac{\beta_1^2}{18}(7(U_0^0)^3 - 11(U_0^0)^2 - 62U_0^0 + 72)\right]\right] Re_1\sqrt{Da_1} \quad (45)$$

and

$$U_0 = U_0^0 + \delta_1 U_0^1 + \delta_1^2 U_0^2. \quad (46)$$

Using a double perturbation expansion, the temperature field is expanded in terms of $(Pr_1)^{-1/2}$ as

$$\theta_{i1}(\xi, \eta_{iT}) = \theta_0(\xi, \eta_{iT}) + \theta_1(\xi, \eta_{iT})Pr_1^{-1/2} + \theta_2(\xi, \eta_{iT})Pr_1^{-1} + \ldots \quad (47)$$

with the interface temperature expanded as

$$\Delta(\xi) = \Delta_0(\xi) + \Delta_1(\xi) Pr_1^{-1/2} + \dots \quad (48)$$

$$\nabla(\xi) = \nabla_0(\xi) + \nabla_1(\xi) Pr_2^{-1/2} + \dots \quad (49)$$

As mentioned before, the interface temperature itself is solved using continuity conditions. The first- and second-order temperature distributions in the upper domain are found to be

$$\theta_0(\xi, \eta_{iT}) = \left[\frac{1}{1+(r_2 r_5)^{1/2}}\right] \operatorname{erfc}\left(\sqrt{\left(\frac{\psi_1 \eta_{iT}^2}{4\xi}\right)}\right) \quad (50)$$

$$\theta_1(\xi, \eta_{iT}) = \sqrt{\left(\frac{\xi}{\pi}\right)} \exp\left(\frac{-\psi_1 \eta_{iT}^2}{4\xi}\right) \times \left(\omega - \frac{\Lambda_2 \Delta_0}{4\sqrt{\psi_1}} \frac{\eta_{iT}^2}{\xi}\right) - \eta_{iT} \operatorname{erfc}\left(\sqrt{\left(\frac{\psi_1 \eta_{iT}^2}{4\xi}\right)}\right) \times \left(\frac{\omega\sqrt{\psi_1}}{2} + \frac{\Lambda_2 \Delta_0}{4\psi_1}\right) \quad (51)$$

where

$$\omega = \left[\frac{\Lambda_2^*}{2\psi_1^*}(1-\Delta_0) - \sqrt{\left(\frac{r_2 r_5^2}{r_1}\right)} \frac{\Lambda_2 \Delta_0}{2\sqrt{\psi_1}}\right] \Bigg/ \left[\sqrt{(\psi_1^* r_5)} + \sqrt{\left(\frac{r_2 r_5^2}{r_1}\right)} \sqrt{\psi_1}\right] \quad (52)$$

$$\psi_1^* = V_0 Re_2 \sqrt{Da_2} \quad (53)$$

$$\Lambda_2^* = \left[(1-V_0^0) - \delta_2 \left[V_0^1 + \frac{\beta_2}{3}((V_0^0)^2 + V_0^0 + 1)\right] - \delta_2^2 \left[(V_0^0)^2 + \frac{\beta_2 V_0^1}{3}(2V_0^0+1) + \frac{\beta_2^2}{18}(7(V_0^0)^3 - 11(V_0^0)^2 - 62V_0^0 + 72)\right]\right] Re_2 \sqrt{Da_2} \quad (54)$$

$$V_0 = V_0^0 + \delta_2 V_0^1 + \delta_2^2 V_0^2 \quad (55)$$

$$\Delta_0 = [1+(r_2 r_5)^{1/2}]^{-1} \quad (56)$$

$$\nabla_0 = [1+(r_2 r_5)^{-1/2}]^{-1}. \quad (57)$$

A similar solution can also be written for the lower porous medium. The analysis reveals that for the high Prandtl number fluids, the interface temperature does vary with ξ. Therefore, in contrast to the low Prandtl number fluids the interface temperature is a function of the downstream distance for high Prandtl number fluids.

4.3. *Interface region between two porous media with surface heat generation at the interface*

This case can correspond to some energy related problems, such as, underground coal gasification. The surface heat generation will lead to a temperature distribution along the interface. To consider a somewhat general case, this surface temperature variation is denoted by a power law variation such as $B\xi^q$. The analysis and solution procedure for this problem are similar to those for a porous medium with an impermeable boundary. For this case, only the results for the upper porous medium are given. For the low Prandtl number fluids the solution inside the TBL is obtained in terms of the Whitaker function as

$$\theta_{i1}(\xi, \eta_{iT}) = \frac{\Gamma(q+1)}{\sqrt{\pi}} \left(\frac{\Omega_1 \eta_{iT}^2}{4\xi}\right)^{-1/4} (B\xi^q) \times \exp\left(-\frac{1}{2}\frac{\Omega_1 \eta_{iT}^2}{4\xi}\right) W_{-q-1/4,1/4}\left(\frac{\Omega_1 \eta_{iT}^2}{4\xi}\right). \quad (58)$$

For very large Prandtl numbers, the temperature distribution in the upper porous medium inside the TBL is obtained in a different form but still in terms of the Whitaker function, W, as

$$\theta_{i1}(\xi, \eta_{iT}) = B\xi^q \frac{\Gamma(q+1)}{\sqrt{\pi}} \left(\frac{\psi_1 \eta_{iT}^2}{4\xi}\right)^{-1/4} \times \exp\left(-\frac{\psi_1 \eta_{iT}^2}{8\xi}\right) W_{-q-1/4,1/4}\left(\frac{\psi_1 \eta_{iT}^2}{4\xi}\right). \quad (59)$$

4.4. *Interface region between a porous medium and a fluid*

The schematic for this case is shown in Fig. 1(b). For high Prandtl number fluids, the temperature field outside the TBLs in the fluid and the porous medium attains the free stream values $T_{\infty,1}$ and $T_{\infty,2}$, respectively. Again, the analysis and solution procedure for this problem are similar to those for two porous media with different properties. The temperature fields T_1, and $\langle T_2 \rangle$ in the channel and the porous medium are nondimensionalized as

$$\theta_{c1} = \frac{T_1 - T_{\infty,1}}{T_{\infty,2} - T_{\infty,1}}$$

$$\theta_{c2} = \frac{\langle T_2 \rangle - T_{\infty,2}}{T_{\infty,1} - T_{\infty,2}}.$$

Again the expansions for the above temperatures and the interface temperature are written as

$$\theta_{c1} = \theta_{c0} + \theta_{c1} Pr_1^{-1/2} + \dots \quad (60)$$

$$\theta_{c2} = \theta_{c0}^* + \theta_{c1}^* Pr_2^{-1/2} + \dots \quad (61)$$

$$\Delta_c = \Delta_{c0} + \Delta_{c1} Pr_1^{-1/2} + \dots \quad (62)$$

$$\nabla_c = \nabla_{c0} + \nabla_{c1} Pr_2^{-1/2} + \dots \quad (63)$$

The first- and second-order temperature distributions in the channel region are found to be

$$\theta_{c0}(\xi, \eta_{cT}) = \left[\frac{\delta^{1/2}}{\delta^{1/2} + r_5^{1/2}}\right] \operatorname{erfc}\left(\sqrt{\left(\frac{\psi_{c1}^* \eta_{cT}^2}{4\xi}\right)}\right) \quad (64)$$

$$\theta_{c1}(\xi,\eta_{cT}) = \sqrt{\left(\frac{\xi}{\pi}\right)}\exp\left(\frac{-\psi_{c1}^{*}\eta_{cT}^{2}}{4\xi}\right)$$
$$\times\left(\Omega-\frac{\Lambda_{c2}\Delta_{c0}}{4\sqrt{\psi_{c1}^{*}}}\frac{\eta_{cT}^{2}}{\xi}\right)-\eta_{cT}\,\mathrm{erfc}\left(\sqrt{\left(\frac{\psi_{c1}^{*}\eta_{cT}^{2}}{4\xi}\right)}\right)$$
$$\times\left(\frac{\Omega\sqrt{\psi_{c1}^{*}}}{2}+\frac{\Omega_{c2}^{*}\Delta_{c0}}{4\psi_{c1}^{*}}\right) \quad (65)$$

and the first- and second-order temperature distributions in the porous medium are found to be

$$\theta_{c0}^{*}(\xi,\eta_{cT}^{*}) = \left(\frac{1}{1+\delta^{1/2}r_5^{-1/2}}\right)\mathrm{erfc}\left(\sqrt{\left(\frac{\psi_{c1}^{*}\eta_{cT}^{*2}}{4\xi}\right)}\right) \quad (66)$$

$$\theta_{c1}^{*}(\xi,\eta_{cT}^{*}) = \sqrt{\left(\frac{\xi}{\pi}\right)}\exp\left(-\frac{\psi_{c1}^{*}\eta_{cT}^{*2}}{4\xi}\right)$$
$$\times\left(\phi-\frac{\Lambda_{c2}\nabla_{c0}}{4\psi_{c1}^{*1/2}}\frac{\eta_{cT}^{*2}}{\xi}\right)-\eta_{cT}^{*}\,\mathrm{erfc}\left(\frac{\psi_{c1}^{*}\eta_{cT}^{*2}}{4\xi}\right)$$
$$\times\left(\frac{\phi\sqrt{\psi_1^{*}}}{2}+\frac{\Delta_{c2}^{*}\nabla_{c0}}{4\psi_{c1}^{*}}\right). \quad (67)$$

Here η_{cT} and η_{cT}^{*} are non-dimensional normal coordinates for the channel and the porous region which are given respectively by $y_1/\sqrt{(K/Pr_1)}$ and $y_2/\sqrt{(K/\delta\,Pr_2)}$ and

$$\psi_{c1}^{*} = U_0\,Re_{ch}\sqrt{Da} \quad (68)$$

$$\Lambda_{c2}^{*} = -\left[\varepsilon_{cM}+\varepsilon_{cM}^{2}+\left((\delta+1)\alpha-2\delta+1+\frac{4}{9}\alpha^{2}\right)\varepsilon_{cM}^{3}\right]$$
$$\times Re_{ch}\sqrt{Da} \quad (69)$$

$$\Lambda_{c2} = (1-U_0)\sqrt{\left(\frac{K}{h^{2}}\right)}Re_{ch}\sqrt{Da} \quad (70)$$

$$\Delta_{c0} = [1+\delta^{-1/2}r_5^{1/2}]^{-1} \quad (71)$$

$$\nabla_{c0} = [1+\delta^{1/2}r_5^{-1/2}]^{-1} \quad (72)$$

$$\Omega = \left[\frac{\Lambda_{c2}^{*}}{2\psi_{c1}^{*}}(1-\Delta_{c0})-\frac{r_5}{\delta^{1/2}}\frac{\Lambda_{c2}\Delta_{c0}}{2\psi_{c1}^{*}}\right]\Bigg/$$
$$\left[\sqrt{(\psi_1^{*}r_5)}+\frac{r_5}{\delta^{1/2}}\sqrt{\psi_{c1}^{*}}\right] \quad (73)$$

$$\phi = \left[r_5\delta^{-1/2}\frac{\Lambda_{c2}}{2\psi_{c1}^{*}}(1-\nabla_{c0})-\frac{\Lambda_{c2}^{*}}{2\psi_{c1}^{*}}\nabla_{c0}\right]\Bigg/$$
$$[\psi_1^{*1/2}+r_5^{1/2}\delta^{-1/2}\psi_{c1}^{*}]. \quad (74)$$

For this case, as in the case of the interface between two porous media, the interface temperature is found to be dependent on ξ.

5. NUSSELT NUMBERS FOR DIFFERENT INTERFACE REGIONS

In this section explicit analytical expressions are obtained for the heat flux at the interface for all three cases. These expressions are obtained in part from the theoretical analysis which was done in the previous section. The heat flux quantities are then expressed in the non-dimensional form as the Nusselt numbers.

First considering the interface between an impermeable medium and a permeable medium the Nusselt number is derived for the low and high Prandtl number fluids. For the low Prandtl number fluids the Nusselt number is obtained as

$$Nu_{\xi} = \left(\frac{Pr\,\delta}{Da}\right)^{1/2}\sqrt{\Omega}\,\frac{\Gamma(p+1)}{\Gamma(p+1/2)}\xi^{1/2} \quad (75)$$

where Γ is the gamma function. For the high Prandtl number fluids the Nusselt number is obtained as

$$Nu_{\xi} = \frac{3^{1/3}\Gamma(2/3)}{\Gamma(1/3)}\frac{\Gamma(p+1)}{\Gamma(p+2/3)}\lambda^{1/3}\left(\frac{Pr\,\delta}{Da}\right)^{1/2}\xi^{2/3} \quad (76)$$

where, as mentioned before, λ is a parameter which is explicitly related to the friction factor, Reynolds number, porosity, Darcy number, and the Prandtl number, whereas Ω is not dependent on the Prandtl number. The analysis shows that for high Prandtl number fluids the Nusselt number is proportional to $Pr^{1/3}$ and for low Prandtl number fluids the Nusselt number is proportional to $Pr^{1/2}$. As it becomes evident in the next section the Nusselt number expressions are extremely accurate even for Prandtl numbers where the analytical temperature distribution shows some deviations. This is because the analytical temperature distribution is extremely accurate close to the interface region even for Prandtl numbers where the temperature distribution deviates slightly outside the interface region. However, it should be mentioned that the temperature distributions, in general, are also very accurate and the deviations, if any, are quite small.

The Nusselt number for the interface region between two different porous media with different free stream temperatures is also derived for the low and high Prandtl number fluids based on the temperature distributions that were derived in the previous section. For the low Prandtl number fluids the Nusselt number is obtained as

$$Nu_{\xi} = \left(\frac{Pr_1\,\delta_1}{Da_1}\right)^{1/2}\sqrt{\left(\frac{\Omega_1}{\pi}\right)}\xi^{1/2}. \quad (77)$$

It should be noted that the ξ dependence for the low Prandtl number fluids is the same for the two types of interfaces.

For the high Prandtl number fluids the Nusselt number for the interface region between two different porous media with different free stream temperatures is obtained as

$$Nu_\xi = \left[\Delta_0\psi_1^{1/2}\,Pr_1^{1/2} + \left(\frac{\psi_1^{1/2}\omega}{2} - \frac{\Lambda_2\Delta_0}{4\psi_1}\right)\pi\xi^{1/2}\right] \Big/ \left[\left(\omega\,Pr_1^{-1/2} + \Delta_0\left(\frac{\pi}{\xi}\right)^{1/2}\right)(\delta_1\,Da_1)^{1/2}\right]. \quad (78)$$

For the interface region between a high Prandtl number fluid and a porous medium the Nusselt number is found to be

$$Nu_\xi = \left[\Delta_{c0}\psi_{c1}^{*1/2}\,Pr_1^{1/2} + \left(\frac{\psi_{c1}^{*1/2}\Omega}{2} - \frac{\Lambda_{c2}\Delta_{c0}}{4\psi_{c1}^{*}}\right)\pi\xi^{1/2}\right] \Big/ \left[\left(\Omega\,Pr_1^{-1/2} + \Delta_{c0}\left(\frac{\pi}{\xi}\right)^{1/2}\right)(\delta\,Da)^{1/2}\right]. \quad (79)$$

6. RESULTS AND DISCUSSIONS

In this section the flow and heat transfer results for different types of interface conditions are discussed. The analytical solutions for the velocity and temperature distributions are compared with the corresponding numerical solutions for different interface conditions. The explicit expression for the interface velocity for the case of the interface region between a porous medium and a fluid, which was derived theoretically, is compared with the pseudo interface velocity extracted from the Beavers and Joseph model [21] as well as the numerical results.

The numerical results are obtained by finite differencing the governing equations. A central differencing scheme is used to evaluate the second derivatives while the non-linear terms are replaced by a suitable linearized approximation. The analytical solutions for the velocity distributions are evaluated from the corresponding theoretical results presented in Section 3. The analytical temperature distributions are obtained by evaluating the explicit theoretical results presented in Section 4.

Figure 3 compares the analytical and the numerical solutions for the interface region between two different porous media for $Re_1 = 0.1$, 2 and 3. The upper porous medium physical properties were chosen as: $K_1 = 10^{-7}\,m^2$, $F_1 = 0.07$ and $\delta_1 = 0.98$. The property ratios r_1, r_2, and r_3 used in Fig. 3 were 2, 1.5 and 1, respectively. The analytical and numerical solutions are seen to be in quite good agreement. It has been found through numerous numerical experimentation that reasonable agreement between the numerical and analytical results is obtained for many practical situations.

Figure 4 presents the velocity distributions for the interface region between an impermeable medium and a porous medium. The velocity distributions are presented for two different Reynolds numbers which are $Re_1 = 0.1$ and 3. As it can be seen, although the agreement in general is good, it is better for lower Reynolds numbers. It should be noted that the results of the interface region between two porous media and the

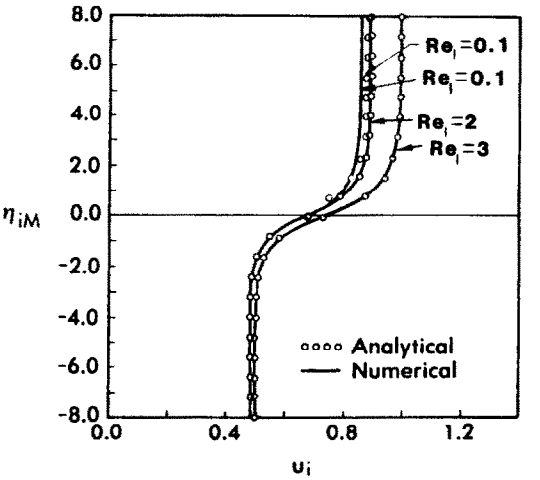

FIG. 3. The velocity distribution for the interface region between two different porous media for $Re_1 = 0.1$, 2, and 3 and property ratios $r_1 = 2$, $r_2 = 1.5$ and $r_3 = 1$.

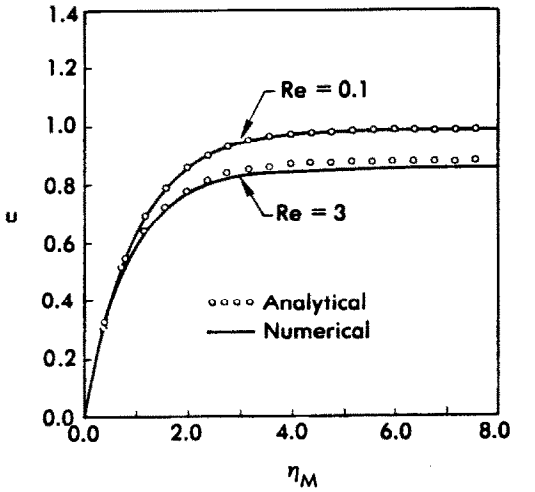

FIG. 4. The velocity distributions for $Re = 0.1$ and 3 for the interface region between a porous medium and an impermeable medium.

interface region between an impermeable medium and a porous medium can very easily combine to produce the velocity distribution inside a bounded channel filled with two different porous media. The complete velocity distribution inside the bounded channel for the same property ratios as in Fig. 3 is shown in Fig. 5 for two different Reynolds numbers. As it can be seen in Fig. 5 inside the channel four distinct boundary layers exist. These are the two boundary layers along the two impermeable boundaries and the two boundary layers interconnected at the interface along each of the two porous media. Furthermore, the results obtained in Sections 3 and 4 can be easily combined to produce the velocity and temperature distributions in a multi-layered porous medium as for example the flow of oil in different layers of sand, rock, shale and limestone.

The explicit analytical expression for the interface

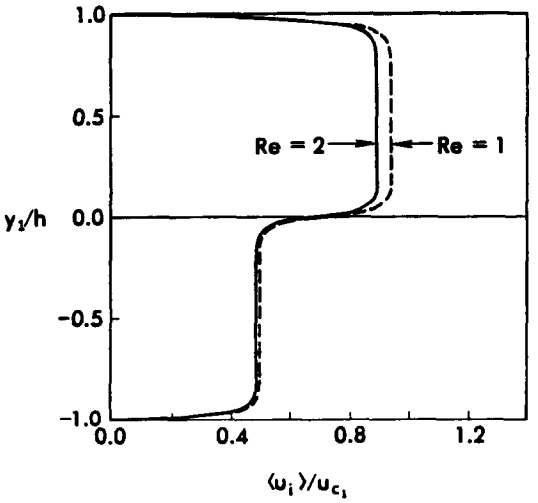

FIG. 5. The complete velocity distribution inside a bounded channel filled with two different porous media for $Re_1 = 1$ and 2.

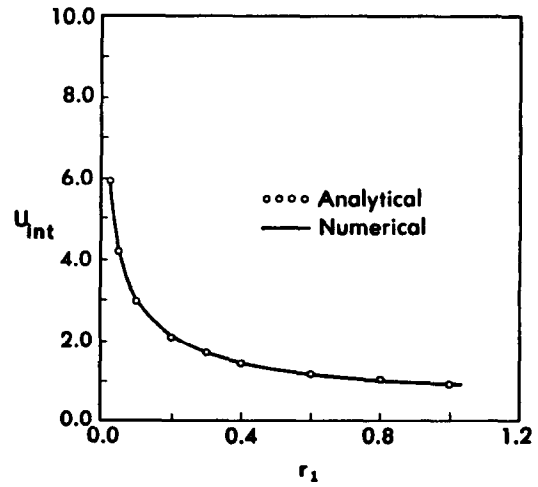

FIG. 6. The variations of the interface velocity between two porous media as a function of their corresponding permeability ratios.

velocity for the interface region between two different porous media is compared with the numerical results in Fig. 6. In the numerical runs, to obtain an accurate value for the interface velocity, the number of grid points and successive iterations are increased till convergence is achieved. In the theoretical analysis the interface velocity was uniquely determined by the material properties of the two porous media and the flow parameters.

The variations of the interface velocity for different values of the permeability ratios are presented in Fig. 6. The material properties of the upper porous medium used in this figure were $K_1 = 10^{-9}\,\mathrm{m}^2$, $\delta_1 = 0.7$ and $F_1 = 0.07$ and the property ratios were $r_2 = 0.9$, $r_3 = 1$. As it can be seen from Fig. 6 the agreement between the numerical result and the explicit analytical expression for the interface velocity is excellent. Furthermore, the variations of the interface velocity is in accordance with physical principles. From numerous numerical experimentations it is found that the interface velocity decreases when r_1 is increased because the permeability of the lower porous medium is decreased. The interface velocity will tend asymptotically towards zero when both the permeability and the porosity of the lower porous medium tend towards zero. This represents the limiting case of the lower medium being an impermeable solid boundary. On the other hand since r_3 is the ratio of the friction functions F_1 and F_2, an increase in r_3 implies a decrease in F_2, which in turn signifies a decrease in the resistance offered by the porous structure. This influences the interface velocity directly as the overall flow in the lower porous medium increases causing an increase in the interface velocity.

Next, the explicit theoretical expression for the interface velocity obtained from the present analytical work for the interface region between a fluid region and a porous medium is compared with the empirical model proposed by Beavers and Joseph [21] which states that the velocity gradient at the interface is proportional to the difference between the slip velocity and the Darcian convective velocity. For purposes of comparison, a new parameter is introduced, namely

$$\sigma = h/\sqrt{K}. \tag{80}$$

Beavers and Joseph proposed that the interface condition is given by

$$\frac{\mathrm{d}u_\mathrm{f}}{\mathrm{d}y_1} = \frac{\alpha^*}{\sqrt{K}}(u_\mathrm{f} - u_\mathrm{c}) \quad \text{at the interface} \tag{81}$$

where

$\alpha^* \equiv$ the proportionality constant

$u_\mathrm{c} = -\dfrac{K}{\mu_\mathrm{f}}\dfrac{\mathrm{d}p}{\mathrm{d}x}$ is the Darcian convective velocity

$u_\mathrm{f} =$ fluid velocity.

Based on their proposed shear condition the following quantity

$$U_{\mathrm{int,exp}} = \frac{\sigma + 2\alpha^*}{\sigma(1+\alpha^*\sigma)} \tag{82}$$

can be obtained as the interface velocity.

In what follows for a given value of σ, the analytical interface velocity, the numerical interface velocity (based on the numerical solution of the governing equations) and the interface velocity from the empirical results of ref. [21] are computed and compared for the same pressure gradient and in the linear regime which was used in the Beavers and Joseph experiments. The results of such a comparison are given in Table 1. Upon examining Table 1 it can be seen that the analytical interface velocity, the numerical interface velocity and the pseudo-interface velocity obtained from Beavers and Joseph are in excellent

Table 1. Comparison between the analytical, numerical and empirical interface velocities

$\sigma = h/\sqrt{K}$	$U_{int,A}$ (from the explicit analytical expression)	$U_{int,N}$ (numerical solution of the governing equations)	$U_{int,exp}$ (interface velocity obtained from the experimental results)
4	0.3045	0.2940	0.2940
8	0.1438	0.1436	0.1436
12	0.0935	0.0935	0.0935
16	0.0691	0.0691	0.0691
20	0.0548	0.0548	0.0548
24	0.0454	0.0454	0.0454
28	0.0387	0.0387	0.0387
32	0.03378	0.03378	0.03379
36	0.02995	0.02995	0.02996
40	0.02689	0.02689	0.02690
44	0.02440	0.02441	0.02442
48	0.02234	0.02234	0.02235
52	0.02059	0.02060	0.02060
56	0.01910	0.01911	0.01911
60	0.01781	0.01782	0.01782
64	0.01668	0.01669	0.01669
68	0.01569	0.01570	0.01570
72	0.01481	0.01482	0.01482
76	0.01402	0.01403	0.01403
80	0.01331	0.01332	0.01332
84	0.01267	0.01268	0.01268
88	0.01209	0.01210	0.01210
92	0.01156	0.01157	0.01157
96	0.01108	0.01108	0.01109
100	0.01063	0.01064	0.01064

agreement. Furthermore, the results of the analysis given in Table 1 confirm the hypothesis proposed by Beavers and Joseph, namely, the velocity gradient at the interface is proportional to the difference between the slip velocity and the Darcian convective velocity within the porous medium.

The temperature profiles for the interface region between an impermeable and a porous medium are shown in Figs. 7–9. For all these figures a linear surface temperature variation is assumed. All of the results are presented at $\xi = 1$ except in Fig. 9. Figure 7(a) presents the temperature profiles for low Prandtl number fluids at three different Reynolds numbers. These are $Re = 0.1$, 1 and 10. As expected, the higher the Prandtl number the thinner the thermal boundary layer. As seen in Fig. 7(a) the agreement between the analytical and numerical results is excellent. Figure 7(b) presents a comparison between the theoretical results for the low Prandtl number fluid and the numerical results for two Prandtl numbers 0.73 and 8. Again the agreement is excellent. It is worth noting that the low Prandtl number solution predicts accurately the temperature distribution even for a Prandtl number as high as 8.

In Fig. 8(a), the high Prandtl number analytical results are compared with the numerical results at three different Reynolds numbers. All other factors being the same, higher velocities lead to thinner thermal boundary layers. Also as seen in Fig. 8(a), the agreement between the analytical and numerical results is quite good. Figure 8(b) shows the temperature profiles at three different Prandtl numbers. As expected the higher the Prandtl number the thinner the thermal boundary layer. As seen in Fig. 8(b) the agreement between the analytical and numerical results is not good for Prandtl numbers around eight. However, since the low Prandtl number solution easily covers Prandtl numbers around eight, it can be said that the two Prandtl regimes cover most of the practical situations.

For the cases where the theoretical temperature distribution is not in excellent agreement with the numerical results the theoretical Nusselt number

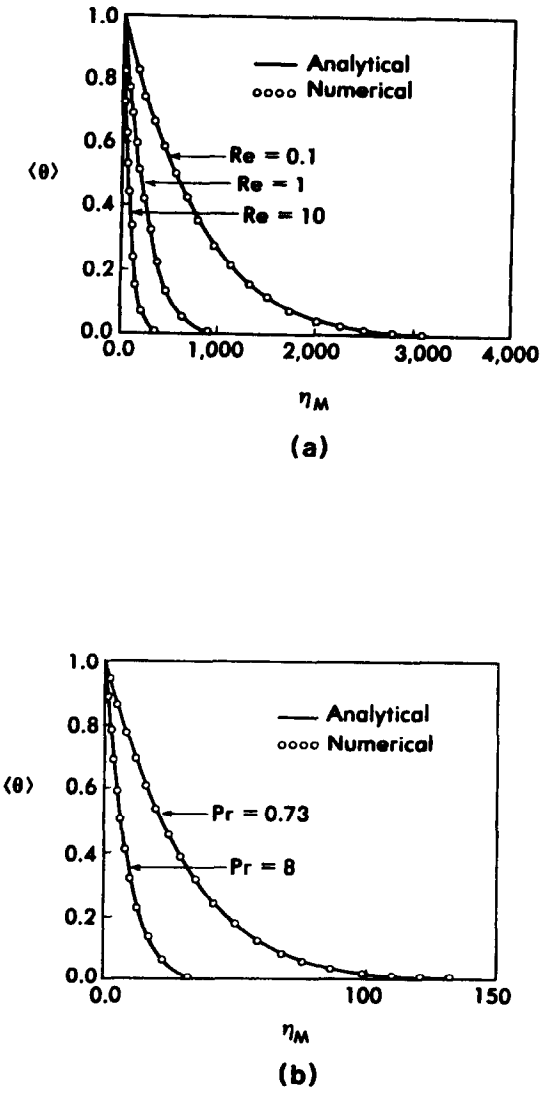

FIG. 7. (a) Comparison between the analytical and numerical temperature distributions for a low Prandtl number fluid at three different Reynolds numbers for the interface region between an impermeable medium and a permeable medium. (b) Prandtl number effect on the low Prandtl number analytical temperature distribution.

results are still found to be in excellent agreement with the numerical results. This fact becomes apparent upon closer examination of Fig. 8. The temperature profiles at different locations are presented in Fig. 9. It should be noted that the temperature is non-dimensionalized with respect to the temperature difference between the surface and free stream at $\xi = 1$. This type of nondimensionalization causes a downshift in the temperature profiles as seen in Fig. 9. Again as seen in Fig. 9 there is excellent agreement between the analytical results for high Prandtl number fluids and the numerical results.

Finally the comparison between the experimental, theoretical and numerical interface velocity, given in Table 1, is plotted also in Fig. 10. Again, it can be seen that there is an excellent agreement between the theoretical and experimental results.

A major advantage of the present work is that the analytical solutions which are presented here can be of significant help in refining the equations for the porous media. This is because these fundamental analytical solutions can be easily used to readily analyze the functional dependencies and the effects of the different coefficients and properties of the porous media in the governing equations, thereby enabling a more accurate correlation and evaluation of the future experimental studies.

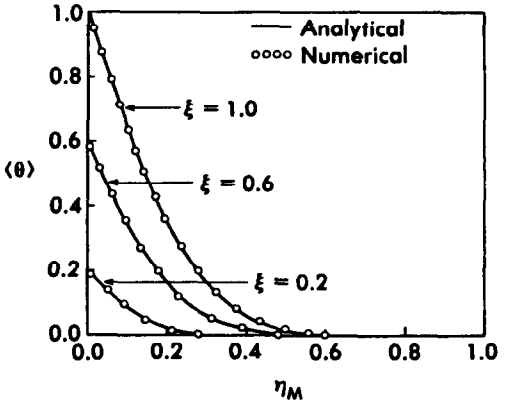

FIG. 9. Temperature distributions at different downstream locations.

7. CONCLUSIONS

A complete and thorough analysis of the fluid flow and heat transfer at the interface region of a porous medium is presented. The physics of the interface region is discussed in detail for three general and fundamental classes of problems in porous media. Theoretical solutions are obtained for the velocity and temperature distributions for all cases. Explicit expressions for the interface velocity and temperature can be easily obtained for all cases from the theoretical solutions. The theoretical solutions are shown to be in excellent agreement with the numerical results. The analytical results are also checked against an empirically based hypothesis for the interface region between a fluid and a porous medium and are found to be in excellent agreement.

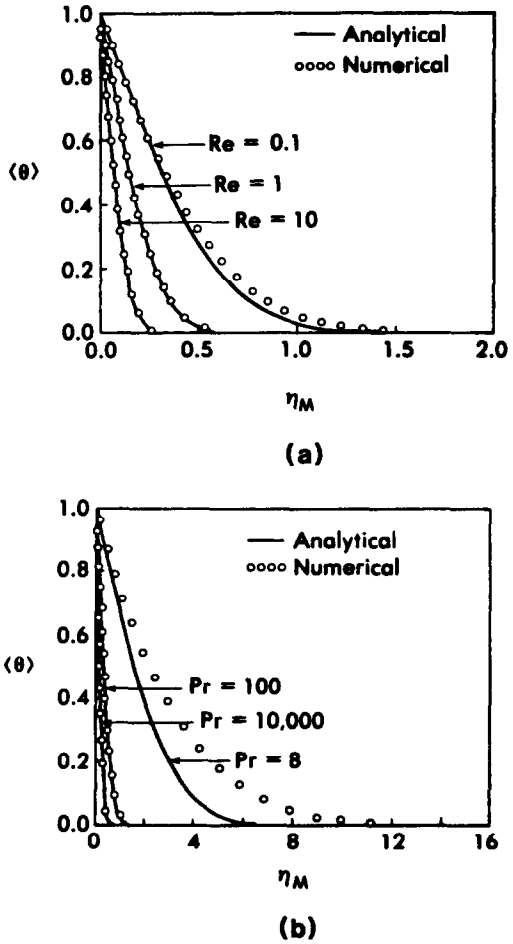

FIG. 8. (a) Comparison between the high Prandtl number analytical solution and the numerical results for different flow regimes. (b) The variations of the Prandtl number on the high Prandtl number analytical solution.

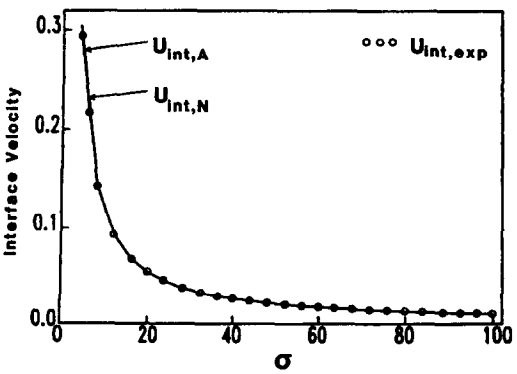

FIG. 10. Comparison between the empirically based interface velocity with the theoretical and numerical interface velocity.

Acknowledgement—The authors are grateful to Mrs Barbara G. Dole for her excellent work in typing this manuscript.

REFERENCES

1. P. Cheng, Heat transfer in geothermal systems, *Adv. Heat Transfer* **14,** 1–105 (1978).
2. P. Cheng and J. Minkowycz, Free convection about a vertical flat plate embedded in a porous medium with application to heat transfer from a dyke, *J. Geophys. Res.* **82,** 2040–2044 (1977).
3. K. Vafai and C. L. Tien, Boundary and inertia effects on flow and heat transfer in porous media, *Int. J. Heat Mass Transfer* **24,** 195–203 (1981).
4. M. Kaviany, Laminar flow through a porous channel bounded by isothermal parallel plates, *Int. J. Heat Mass Transfer* **28,** 851–858 (1985).
5. C. T. Hsu and P. Cheng, The Brinkman model for convection about a semi-infinite vertical flat plate in a porous medium, *Int. J. Heat Mass Transfer* **28,** 683–697 (1985).
6. C. L. Tien and M. L. Hunt, Boundary-layer flow and heat transfer in porous beds, *Chem. Engng Processing* **21,** 53–63 (1987).
7. M. Kaviany, Thermal convective instabilities in a porous medium, *J. Heat Transfer* **106,** 137–142 (1984).
8. J. T. Hong, C. L. Tien and M. Kaviany, Non-Darcian effects on vertical-plate natural convection in porous media with high porosities, *Int. J. Heat Mass Transfer* **28,** 2149–2157 (1985).
9. T. W. Tong and E. Subramanian, A boundary-layer analysis for natural convection in vertical porous enclosures—use of the Brinkman-extended Darcy-model, *Int. J. Heat Mass Transfer* **28,** 563–571 (1985).
10. K. Vafai and C. L. Tien, Boundary and inertia effects on convective mass transfer in porous media, *Int. J. Heat Mass Transfer* **25,** 1183–1190 (1982).
11. P. Ranganathan and R. Viskanta, Mixed convection boundary-layer flow along a vertical surface in a porous medium, *J. Numer. Heat Transfer* **7,** 305–317 (1984).
12. M. L. Hunt and C. L. Tien, Non Darcian convection in cylindrical packed beds, ASME–JSME Conference (1987).
13. K. Vafai, Convective flow and heat transfer in variable porosity media, *J. Fluid Mech.* **147,** 233–259 (1984).
14. D. A. Nield, The boundary corrections for the Rayleigh–Darcy problem: limitations of the Brinkman equation, *J. Fluid Mech.* **128,** 37–46 (1983).
15. D. A. Nield, Non-Darcy effects in convection in a saturated porous medium, *Proceedings of Institute of Physical Sciences*, Wairakei, New Zealand (1984).
16. D. Poulikakos and A. Bejan, The departure from Darcy flow in natural convection in a vertical porous layer, *Physics Fluids* **28,** 3477–3484 (1985).
17. M. Kaviany, Gradient destruction in flow through a rigid matrix, *J. Fluid Mech.* **165,** 221–230 (1986).
18. K. Vafai, R. L. Alkire and C. L. Tien, An experimental investigation of heat transfer in variable porosity media, *J. Heat Transfer* **107,** 642–647 (1985).
19. R. Friedrich and N. Rudraiah, Similarity solutions of Brinkman equations for a two-dimensional plane jet in a porous medium, *J. Fluids Engng* **105,** 474–478 (1983).
20. J. G. Georgiadis and I. Catton, Free convective motion in an infinite vertical porous slot: the non-Darcian regime, *Int. J. Heat Mass Transfer* **28,** 2389–2392 (1985).
21. G. S. Beavers and D. D. Joseph, Boundary conditions at a naturally permeable wall, *J. Fluid Mech.* **30,** 197–207 (1967).
22. S. Whitaker, Advances in theory of fluid motion in porous media, *Ind. Engng Chem.* **61,** 14–28 (1969).
23. S. Whitaker, Diffusion and dispersion in porous media, *A.I.Ch.E. Jl.* **13,** 420–427 (1967).
24. R. Thiyagaraja, Interface interaction in fluid flow through a two layered porous medium, Thesis, Ohio State University, Columbus, Ohio (1985).

ANALYSE DE L'ECOULEMENT ET DU TRANSFERT THERMIQUE DANS LA REGION INTERFACIALE D'UN MILIEU POREUX

Résumé—L'écoulement d'un fluide et le transfert de chaleur dans la région interfaciale sont analysés pour trois classes fondamentales de problèmes concernant les milieux poreux: la région interfaciale entre deux milieux poreux différents, entre la zone fluide et le milieu poreux et entre un milieu imperméable et un milieu poreux. Ces trois types de régions interfaciales recouvrent complètement les interactions d'interface dans un milieu poreux saturé. Des solutions analytiques détaillées, à la fois pour les distributions de vitesse et de température sont obtenues pour ces conditions. Les résultats numériques et analytiques sont en bon accord. Ces résultats sont aussi mis à l'épreuve d'hypothèses empiriques pour une des conditions à l'interface, celle de la jonction d'une zone de fluide et d'un milieu poreux, et ils sont en excellent accord avec les hypothèses déduites de l'expérience.

UNTERSUCHUNG VON STRÖMUNG UND WÄRMEÜBERGANG AN GRENZFLÄCHEN VON PORÖSEN MEDIEN

Zusammenfassung—Strömung und Wärmeübergang an Grenzflächen von porösen Medien werden für drei grundlegende Fälle detailliert untersucht. Die Fälle sind: die Grenzfläche zwischen zwei verschiedenen porösen Medien, zwischen einem Fluid und einem porösen Medium und zwischen einem porösen Medium und einer undurchlässigen Wand. Die Untersuchung dieser drei Arten von Grenzflächen deckt alle in einem gesättigten porösen Medium vorkommenden Grenzflächen ab. Analytische Lösungen für Geschwindigkeits- und Temperaturverteilungen werden für alle Grenzflächen hergeleitet. Numerische und analytische Ergebnisse stimmen sehr gut überein. Die numerischen und analytischen Ergebnisse werden auch mit einer auf Versuchsergebnissen beruhenden Hypothese für eine der drei Grenzflächen zwischen porösem Medium und Flüssigkeit verglichen. Die Übereinstimmung ist ausgezeichnet.

АНАЛИЗ ТЕЧЕНИЯ И ТЕПЛОПЕРЕНОСА НА ГРАНИЦЕ РАЗДЕЛА В ПОРИСТОЙ СРЕДЕ

Аннотация—Исследуется течение жидкости и теплоперенос на границе раздела в пористой среде для трех общих основных классов задач: между двумя пористыми средами, между жидкостью и пористой средой, между непроницаемой и пористой средами. Указанные типы граничных областей достаточны для полного исследования взаимодействий на границе в насыщенной пористой среде. Для всех вышеуказанных случаев условий на границе получены подробные аналитические решения для распределений скорости и температуры. Численные и аналитические результаты хорошо согласуются. При проверке полученных результатов с эмпирическими данными для одного из случаев граничных условий, а именно жидкости и пористой среды, получено хорошее соответствие.